Journal of Respiratory Biology and Translational Medicine

SCIEPublish

Article

Cell-Specific Epithelial Senescence in Human Trisomy 21: Implications for Impaired Lung Development

Emerson Kopsack [1], Gabriella Hisoire [1], Joselynn Wallace [2,3], Ian A. Glass [4], Birth Defects Research Laboratory (BDRL) [4,5], Alper Uzun [6,7,8], Phyllis A. Dennery [6,9] and Hongwei Yao [1,9,10,*]

[1] Providence VA Medical Center, Providence, RI 02908, USA; emerson_kopsack@brown.edu (E.K.); gabriella_hisoire@brown.edu (G.H.)
[2] Center for Computational Biology of Human Disease, Brown University, Providence, RI 02912, USA; joselynn_wallace@brown.edu (J.W.)
[3] Center for Computation and Visualization, Brown University, Providence, RI 02912, USA
[4] Department of Pediatrics, University of Washington, Seattle, WA 98195, USA; ianglass@uw.edu (I.A.G.)
[5] Seattle Children's Research Institute, University of Washington, Seattle, WA 98195, USA
[6] Department of Pediatrics, Warren Alpert Medical School of Brown University, Providence, RI 02912, USA; alper_uzun@brown.edu (A.U.); phyllis_dennery@brown.edu (P.A.D.)
[7] Department of Pathology and Laboratory Medicine, Brown University, Providence, RI 02912, USA
[8] Center for Computational Molecular Biology (CCMB), Brown University, Providence, RI 02912, USA
[9] Department of Molecular Biology, Cell Biology and Biochemistry, Brown University, Providence, RI 02912, USA
[10] Department of Medicine, Warren Alpert Medical School of Brown University, Providence, RI 02912, USA

* Corresponding author. E-mail: hongwei_yao@brown.edu (H.Y.)

Received: 5 September 2026; Revised: 14 October 2026; Accepted: 23 October 2026; Available online: 11 November 2026

ABSTRACT: Down syndrome (trisomy 21, T21) is associated with abnormal lung development and features of accelerated biological aging, but the role of cellular senescence in the developing human lung remains unclear. We investigated cellular senescence and associated molecular alterations in human fetal T21 lungs using histological and immunofluorescence analyses, single-cell RNA sequencing, and quantitative proteomics. T21 fetal lungs exhibited impaired branching morphogenesis, increased mesenchymal cellularity, thickened septa, and reduced pulmonary vascularization. Single-cell transcriptomic analysis identified epithelial cells as a major compartment with increased senescence signatures, with significant enrichment in type I alveolar and Club cells. Immunofluorescence confirmed increased $RAGE^+$/lamin $b1^-$ and $RAGE^+/\gamma H2AX^+$ type I alveolar cells as well as $UGRP1^+$/lamin $b1^-$ and $UGRP1^+/\gamma H2AX^+$ Club cells in T21 lungs. T21 epithelial cells showed increased expression of inflammatory and senescence-associated genes, accompanied by suppression of genes involved in epithelial differentiation, developmental signaling, and lung morphogenesis. Proteomic analyses independently demonstrated enrichment of inflammatory, complement, metabolic, extracellular matrix, and cellular stress-related pathways, together with suppression of cell-cycle, DNA replication, DNA repair, and genome-maintenance programs. In conclusion, these findings identify cell-specific epithelial senescence as a prominent molecular and cellular feature of T21 fetal lungs and suggest its potential involvement in impaired pulmonary development.

© 2026 The authors. This is an open access article under the Creative Commons Attribution 4.0 International License (https://creativecommons.org/licenses/by/4.0/).

Keywords: Down syndrome; Cellular senescence; Fetal lung development; Alveolar epithelial cells; Single-cell RNA sequencing

1. Introduction

Down syndrome (DS), caused by the presence of an additional copy of chromosome 21, is the most common chromosomal abnormality compatible with postnatal survival. Although advances in medical care have markedly improved life expectancy, respiratory disease remains a major contributor to hospitalization, morbidity, and mortality in affected individuals [1–3]. Structural abnormalities of the respiratory system, recurrent infections, pulmonary hypertension, and chronic respiratory insufficiency are frequently observed in both children and adults with DS, suggesting that pulmonary abnormalities originate early during development.

Accumulating evidence indicates that the lungs of fetuses with trisomy 21 (T21) undergo abnormal morphogenesis before birth [4–6]. Histological studies have reported simplified airway architecture, altered epithelial differentiation, and impaired vascular development. Consistent with these observations, a recent study using the Dp16 mouse model of DS demonstrated impaired alveolar development, altered inflammatory responses, reduced endothelial angiogenesis, and pulmonary hypertension [7]. Because lung development depends on coordinated interactions among epithelial, mesenchymal, and endothelial compartments, disruption of these developmental programs may have long-lasting consequences for lung function throughout life. However, the molecular mechanisms responsible for these abnormalities remain incompletely understood.

In parallel with developmental defects, DS has increasingly been recognized as a condition associated with accelerated biological aging [8]. Cells carrying an extra copy of chromosome 21 exhibit increased oxidative stress, mitochondrial dysfunction, genomic instability, and altered chromatin organization [9–13]. These abnormalities are known triggers of cellular senescence, a stress-response program characterized by persistent cell-cycle arrest, activation of DNA damage signaling pathways, and acquisition of a pro-inflammatory secretory phenotype. Senescence has been reported in several tissues from individuals with DS [14]. Furthermore, T21 fetal lungs show increased expression of senescence biomarkers (*i.e.*, reduced proliferation and increased senescence-associated secretory phenotype [SASP] gene expression) compared with euploid fetuses [4,15]. A recent study demonstrated elevated senescence markers in developing T21 human lungs [16]. However, cell-specific senescence and its underlying mechanisms are not known.

Cellular senescence may be particularly relevant to fetal lung development because excessive senescence can impair tissue growth, alter intercellular communication, and disrupt organogenesis. Senescent epithelial cells secrete cytokines, chemokines, and matrix-remodeling factors that can influence neighboring endothelial and mesenchymal cells [17]. Therefore, senescence arising during critical stages of lung development may contribute directly to abnormalities in airway branching, alveolar formation, and vascular growth.

In the present study, we combined histological analysis, immunofluorescence, reanalysis of single-cell transcriptomic datasets (GSE272470), and quantitative proteomics to define the cellular and molecular landscape of senescence in human fetal T21 lungs. Our findings demonstrate that senescence is selectively enriched within epithelial populations, particularly type I alveolar cells and Club cells, and is accompanied by activation of inflammatory pathways, suppression of developmental signaling networks, and impaired pulmonary vascular development. These results identify epithelial cell senescence as a previously unrecognized feature of the developing T21 lung and provide new insight into mechanisms that may contribute to pulmonary abnormalities associated with DS.

2. Materials and Methods

2.1. Human Fetal Lung Tissues

Specimens from euploid and T21 fetal (78–145 post-conception days) human lungs were obtained from the Birth Defects Research Laboratory at the University of Washington with ethics board approval and maternal written consent (Table 1). This study was performed in accordance with ethical and legal guidelines of the University of Washington institutional review board.

Table 1. Human samples used in the study.

ID Number	Post-Conception Days	Sex	Aneuploidy	Preservation Method
27449	82	M	Euploid	Snap Frozen
27581	145	M	Euploid	Snap Frozen
28294	135	M	Euploid	Snap Frozen
28470	113	F	Euploid	Snap Frozen
27591	82	M	Euploid	Snap Frozen
29886	103	M	Euploid	Snap Frozen, OCT
29637	105	F	Euploid	Snap Frozen, OCT
29934	125	TBD	Euploid	Snap Frozen, OCT, Paraffin
29943	89	TBD	Euploid	Snap Frozen, OCT, Paraffin
29968	94	M	Euploid	Snap Frozen, OCT, Paraffin
30144	91	F	Euploid	Snap Frozen
24237	82	M	T21	Snap Frozen
24908	145	M	T21	Snap Frozen
25015	113	F	T21	Snap Frozen
28123	135	M	T21	Snap Frozen
28450	82	M	T21	Snap Frozen
29814	127	M	T21	Snap Frozen
29930	78	M	T21	Snap Frozen, OCT, Paraffin
30043	113	M	T21	Snap Frozen, OCT, Paraffin
30008	82	TBD	T21	Snap Frozen, OCT, Paraffin
30151	140	F	T21	Snap Frozen, OCT, Paraffin
30165	94	M	T21	Snap Frozen, OCT, Paraffin
30190	130	F	T21	Snap Frozen, OCT, Paraffin

2.2. Hematoxylin and Eosin (H&E) Staining

For paraffin, slides need to be rehydrated before staining. Slides were incubated in xylene for 5 min two times, and then were dipped 10 times each in 100%, 95%, and 70% ethanol. They were then dipped a few times in tap water before incubating in hematoxylin for 3 min. After 3 min in hematoxylin, slides were washed in running tap water until the water ran clean, then they were dipped in acid alcohol 2–3 times and washed in tap water again. Next, the slides were incubated in ammonium hydroxide for 1 min and then washed with tap water. Slides were finally incubated in eosin Y for 4 s before rehydrating with 10 dips in 95% ethanol, 10 dips in 100% ethanol 3 times, and incubated in xylenes for 1 min 3 times. Images were acquired by an Olympus (Evident) APX100 benchtop fluorescence microscope (Needham, MA, USA).

2.3. Quantification of Mesenchymal Cellularity and Interstitial Thickness

Mesenchymal cellularity, area fraction, and interstitial thickness were quantified in H&E-stained fetal lung sections using Fiji (ImageJ v1.54t, Bethesda, MD, USA), following established principles of quantitative lung morphometry [18,19]. Mesenchymal regions were identified by excluding epithelial structures, vascular lumens, and tissue artifacts. Mesenchymal nuclear density was calculated as the number of hematoxylin-

positive nuclei per unit mesenchymal area (nuclei/mm^2), while mesenchymal area fraction was determined as the proportion of analyzed tissue occupied by mesenchyme. Interstitial thickness was measured as the shortest distance between adjacent epithelial structures across the intervening mesenchyme. Multiple nonoverlapping fields were analyzed per lung, and measurements were averaged to obtain one biological replicate per fetus. Analyses were performed for the pseudoglandular stage (12–13 weeks gestation).

2.4. Immunofluorescence

Paraffin slides were heated at 56° for a few hours to melt paraffin before staining. Slides were deparaffinized with two washes each of xylene, 100% EtOH, 95% EtOH, 70% EtOH, and 50% EtOH for 10 min each wash. This was followed by two 5-min washes in diH_2O. Slides were then boiled in an antigen retrieval buffer for 20 min using a vegetable steamer. After boiling, the slides sat in the buffer for an hour, and were then washed with diH_2O for 5 min. Slides were incubated with a permeabilization buffer twice for 10 min each, followed by blocking for 30 min. After blocking, slides were incubated with primary antibodies (Supplementary Table S1) overnight at 4 °C. The next morning, the primary antibody was removed, and slides were washed twice in permeabilization buffer for 10 min each. Following these washes, slides were incubated with secondary antibodies for 1–2 h, followed by another two washes in a permeabilization buffer for 10 min. Finally, the slides were incubated with 1 µg/mL Hoescht for 5 min, followed by four washes 5 min each with PBS. Coverslips were applied to slides with around 25 µL mounting media.

OCT slides were first fixed in ice cold methanol for 10 min, and then warmed to room temperature and washed twice for 5 min in PBS. Next, slides were washed twice with a permeabilization buffer for 10 min. After the permeabilization buffer, slides were blocked for 30 min and then incubated with primary antibodies overnight at 4 °C. In the morning, slides were washed twice with 1% serum PBS-T and then were incubated with secondary antibodies at room temperature for 1–2 h. Following this incubation, slides were washed twice with 1% serum PBS-T for 10 min. Finally, the slides were incubated with Hoesch (1 µg/mL) for 5 min, followed by two 5-min washes in PBS. Mounting media and coverslips were applied to each slide. Images were acquired by an Olympus (Evident) APX100 benchtop fluorescence microscope.

2.5. Reanalysis of Publicly Available scRNA-Seq and snRNA-Seq Datasets

2.5.1. scRNA-Seq Pre-Processing

We utilized scRNA-seq data from the publicly available datasets with GEO accession numbers GSE272470. All main processing steps were performed with Seurat v.5.0.2 [20]. The quality control steps were performed as described previously [18], retaining cells with between 500 and 10,000 features and less than 25% of reads originating from mitochondrial genes. All figures as part of the scRNA-seq analysis were generated with Seurat v5.0.2 and ggplot2 v3.5.0, all analysis were run in R v4.3.2.

2.5.2. scRNA-Seq Normalization, Integration, and Clustering

Data were normalized and scaled using SCTransform [21], retaining 10,000 variable features. For integration of separate Seurat objects, normalized values from SCTransform and the top variable genes as anchors were applied for reciprocal principal component analysis (RPCA) using the IntegrateLayers() function. The Seurat function FindClusters() with a resolution of 0.1 was used to obtain clusters of cells, and a resolution was set to 0.8 was used to obtain finer-grained sub-clusters of cells.

2.5.3. scRNA-Seq Cell Type Annotation and Senescence Scoring

Cell type annotations and senescence scoring were perfomed using AUCell v1.24 [22]. Genesets for this analysis were obtained through msigdbr v.7.5.1. The DESCARTES_FETAL_LUNG geneset was used for cell type annotations, and the SAUL_SEN_MAYO geneset was used to compute senescence scores.

2.5.4. scRNA-Seq Differential Expression Analysis and Gene Set Enrichment

The Seurat function FindAllMarkers() was used to find marker genes using the SCT assay. Overrepresentation analysis of differentially expressed genes was performed using the clusterProfiler enrichGO() and simplify() functions for GO terms, and enricher() with KEGG genes from msigdb for KEGG terms [23]. The code used for the scRNA-seq data reanalysis is publicly available in the GitHub repository compbiocore/hyao_trisomy.

2.6. Proteomics Assay

2.6.1. S-Trap Digestion and Desalting

Protein lysates (n = 5 per group) were transferred to the custody of the Proteomics Core Facility for proteomic profiling. 100 g of protein from fetal lung tissue, were subjected to S-Trap Micro Digestion and Clean-up (Protifi, Fairport, NY, USA, C02-micro-40) as specified by the manufacturer with some modifications. Approximately 40 L of Lysis Buffer (10% Sodium Dodecyl Sulfate (SDS, Invitrogen, Carlsbad, CA, USA, 15553-035) in 50 mM Triethylammonium Bicarbonate Buffer pH 7.5 (TEAB, Sigma Aldrich, St. Louis, MO, T7408-100ML)) was added to each sample and vortexed for 30 s to bring the total volume to 50 L. Proteins were reduced using Dithiothreitol (DTT, 10 mM final concentration, Sigma Aldrich, St. Louis, MO, USA, 646563-10X.5ML) and incubated at 55 °C for 45 min with mixing. Following denaturation and reduction, samples were alkylated using Iodoacetamide (IAM, 20 mM final concentration, Thermo Scientific, Waltham, MA, USA, A39271) and incubated at room temperature in the dark for 30 min. Following alkylation, samples were acidified using Phosphoric Acid (2.5% final concentration, Sigma Aldrich, St. Louis, MO, USA 79617-250ML), and vortexed for 30 s. 6 volumes of ice-cold Binding Buffer (9 parts LC/MS Grade Methanol (ACROS Organics, Geel, Belgium, 61513-0025):1-part 1M TEAB (100 mM Final concentration)) was added to each sample before the entire sample was transferred to an S-Trap spin column and centrifuged for 30 s at 4000× g. Each sample was then washed three times with 150 L of binding buffer. Following protein washing, 1 vial (20 g) of Trypsin (Promega, Madison, WI, USA, V5111) was reconstituted in 50 mM TEAB and added to each micro spin column to yield a final concentration of 1 g of trypsin for 50 g of protein in 100 L. Samples were then moved to a humidified chamber in a 37 °C incubator and left overnight.

On day 2, samples were left to cool to room temperature for 15 min before 50 L of 50 mM TEAB was added, and each sample was centrifuged for 1 min at 4000× g. Hydrophilic peptides were eluted with 50 L of LC/MS grade Water (Honeywell, Charlotte, NC, USA, 39253-4X2.5L) and 0.1% Formic Acid (Fisher Scientific, Waltham, MA, USA A117-50), and centrifuged again for 1 min at 4000× g. Finally, to elute hydrophobic peptides, 50 L of 50% LC/MS Grade Acetonitrile (Fisher, Waltham, MA, USA A955-4) was added to each sample and allowed to stand for 5 min before being centrifuged for 1 min at 4000× g. Each sample was concentrated using a speed vacuum concentrator (Thermo Fisher Scientific, Waltham, MA, USA) for approximately 90 min. With solvent removed, samples were reconstituted in 5% Acetonitrile and 95% Water with 0.1% Formic Acid.

2.6.2. Data Dependent Acquisition (DDA) LC-MS Proteomic Analysis

Reconstituted peptide samples were separated (one injection per sample) using a Vanquish Neo UHPLC on a 7 cm long (2 cm bed length) 3 m particle size, 100 A, Acclaim PepMap C18 Trap column and IonOpticks Aurora Ultimate 25 cm long × 75 m ID, 1.7 m particle size analytical column throughout a 60-min gradient held at 300 nl/min. Solvent A consisted of Water with 0.1% Formic Acid, and Solvent B consisted of 80% Acetonitrile and 0.1% Formic Acid. The gradient consisted of loading/starting conditions of 5% B, then to 30% B over 50 min followed by 95% B over 5 min, then finishing at 99% B for the remaining 5 min. Combined control was used for loading and washing. Trap column was washed using 4 zebra washes, and the analytical column was washed using 3 alternating aqueous and organic cycles before being re-equilibrated for the next sample injection.

Spray voltage was set to 2050 V, Ion Transfer Tube Temperature was 275 °C, and a user-defined lock mass of 445.12003 was used. MS1 scans used wide quad isolation, orbitrap as the detector with a resolution of 120 K and a mass range of 300–1500 *m*/*z*. A maximum injection time of 50 ms, normalized AGC target of 250%, and an RF Lens set to 30% were selected. Data were collected in centroid mode. MIPS (monoisotopic peak and peptide mode), Charge state (2–7), Precursor Selection Range (375–1500 *m*/*z*), Dynamic Exclusion (exclude after 1 time, 15 s exclusion time, 10 ppm low and high mass tolerance, excluding isotopes), and intensity threshold (intensity range of 20,000 (min)–1E20 (max) with relative intensity threshold of 20%) filters were included. Data-dependent MS2 scans were acquired using a cycle time (3 s), a normalized HCD fragmentation energy of 30%, and a quadrupole isolation width of 0.7 *m*/*z*. Fragments were detected using the Ion Trap with Turbo Mode at a scan range of 150–2000 *m*/*z*. A maximum injection time of 35 ms, normalized AGC target of 100%, and maximum injection time mode of dynamic were used. Data were also collected in centroid mode.

2.6.3. Label Free Quantitation and Spectromine Search Parameters

.raw files were processed using Spectromine (Version 4.4.240326) using 1% peptide and protein FDR search constraints, all settings were system defaults with "single hits removed" option selected against the Human UNIPROT reference FASTA (version 20230316, 42,442 entries canonical + isoform) and Universal Contaminant FASTA file (version 20220701, 381 entries). Variable modifications consisted of oxidation (M), deamidation (N), Acetylation, and protein N-terminal Acetylation. Carbamidomethylation was the sole static modification for the Trypsin search. The exported protein group report was further processed in excel and relative abundance was calculated as the intensity of each protein divided by the sum of all intensities for each given sample.

2.6.4. Proteomics Data Analysis

Differential protein abundance analysis was performed to compare fetal lung samples from T21 and euploid controls. For each protein, the average log2 abundance ratio (T21/Euploid) and corresponding *p* value were used for downstream enrichment analysis. Positive log2 ratios indicated increased protein abundance in T21 fetal lungs, whereas negative log2 ratios indicated decreased abundance. For gene set enrichment analysis (GSEA), a signed ranking metric was calculated for each protein. *p* values were transformed as $-\log_{10}(P)$, and the direction of the score was determined by the sign of the average $\log_2$ abundance ratio: Ranking score $= \text{sign}\left(\text{average } \log_2 \text{ ratio}\right) \times [-\log_{10}(P)]$.

Accordingly, proteins with increased abundance in T21 received positive ranking scores, whereas proteins with decreased abundance received negative ranking scores. Gene symbols and their corresponding signed ranking scores were used to generate a two-column .rnk file containing the complete ranked proteomic dataset. The ranked list was used directly for enrichment analysis without applying a differential-abundance cutoff or separating proteins into increased and decreased subsets. Preranked GSEA was

performed using GSEA v4.3.2 with a weighted enrichment scoring scheme and 1000 permutations. Gene sets containing fewer than 15 or more than 500 genes were excluded. Mean-division normalization was applied, and gene identifiers were analyzed without collapsing.

Gene Ontology (GO) enrichment analysis was performed using human gene sets from the Molecular Signatures Database (MSigDB), including the C5 Biological Process (c5.go.bp.v2025.1.Hs), Cellular Component (c5.go.cc.v2025.1.Hs), and Molecular Function (c5.go.mf.v2025.1.Hs) collections. KEGG pathway enrichment analysis was performed using the MSigDB KEGG Legacy (c2.cp.kegg_legacy.v2024.1.Hs) and KEGG Medicus (c2.cp.kegg_medicus.v2024.1.Hs) collections.

Enrichment results were evaluated using normalized enrichment scores (NES) and false discovery rate (FDR) q-values. Gene sets with an FDR q-value < 0.25 were considered significantly enriched. Positive NES values indicated enrichment toward proteins with increased abundance in T21 fetal lungs, whereas negative NES values indicated enrichment toward proteins with decreased abundance in T21 fetal lungs.

2.7. Statistical Analysis

Statistical analysis was performed using GraphPad Prism 9. Results are displayed as mean ± the standard error of the mean. *t*-Tests were performed to determine statistical significance between 2 groups. p values displayed indicate the following: * $p < 0.05$, ** $p < 0.01$, and *** $p < 0.001$.

3. Results

3.1. Trisomy 21 Disrupts Normal Fetal Lung Architecture

To determine whether tT21 alters fetal lung development, lung sections from euploid and T21 fetuses were examined at 12–13 weeks (pseudoglandular stage) and 16–17 weeks (transition to the canalicular stage) of gestation. Histological analysis revealed distinct architectural abnormalities in T21 lungs compared with euploid controls (Figure 1A). At 12–13 weeks, T21 lungs exhibited fewer epithelial buds, enlarged glandular structures, and increased mesenchymal cellularity, suggesting altered branching morphogenesis. Quantitative analysis confirmed significantly increased mesenchymal nuclear density and interstitial thickness in T21 lungs compared with euploid controls (Figure 1B). At 16–17 weeks, T21 lungs continued to exhibit abnormal epithelial architecture and prominent mesenchymal regions (Figure 1A). These observations suggest that structural abnormalities are present during early fetal lung development and are also evident at later developmental stages.

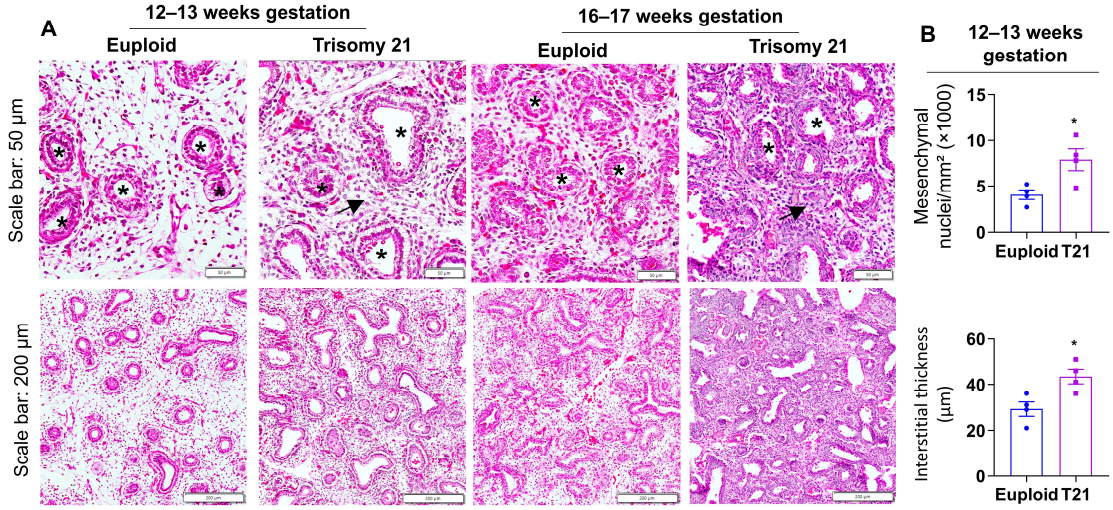


Figure 1. Abnormal lung architecture and increased mesenchymal cellularity in human fetal trisomy 21 lungs. (**A**) Representative H&E-stained lung sections from euploid and trisomy 21 (T21) fetuses at 12–13 and 16–17 weeks of gestation. Compared with

euploid controls, T21 lungs exhibit abnormal epithelial branching, altered airway morphology, increased mesenchymal cellularity, and interstitial thickening. Upper and lower panels show higher- and lower-magnification images, respectively. Asterisks (*) indicate epithelial structures, and arrowheads indicate regions of increased mesenchymal cellularity and interstitial thickening. Scale bars: 50 μm (upper panels) and 200 μm (lower panels). (**B**) Quantification of mesenchymal nuclear density and interstitial thickness in euploid and T21 fetal lungs at 12–13 weeks of gestation. Data are presented as mean ± SEM (n = 4 fetuses per group). * $p < 0.05$ versus euploid controls.

3.2. Pulmonary Vascular Development Is Impaired in Trisomy 21 Lungs

Because airway and vascular development are closely coordinated during lung morphogenesis, endothelial cell abundance was evaluated by immunofluorescence staining for vWF and CD31. Representative images demonstrated fewer vWF-positive vascular structures and reduced CD31-positive endothelial cells in T21 lungs compared with euploid controls at both developmental stages (Figure 2A). Quantitative analysis confirmed a significant reduction in the number of vWF-positive vessels and CD31-positive cells in T21 lungs at 12–13 weeks and 16–17 weeks gestation (Figure 2B). These findings suggest that abnormal epithelial development in T21 is accompanied by impaired pulmonary vascular growth.

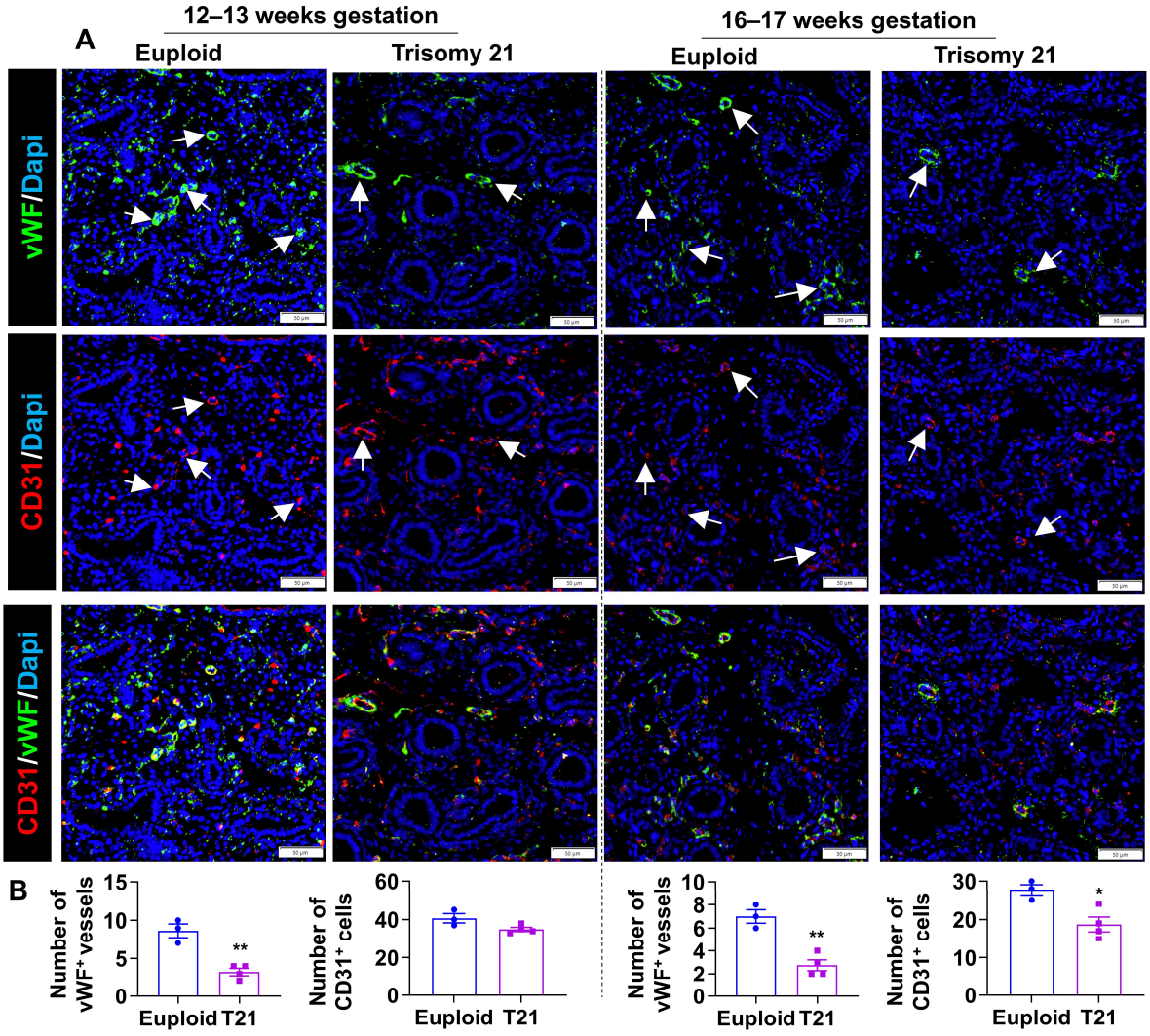
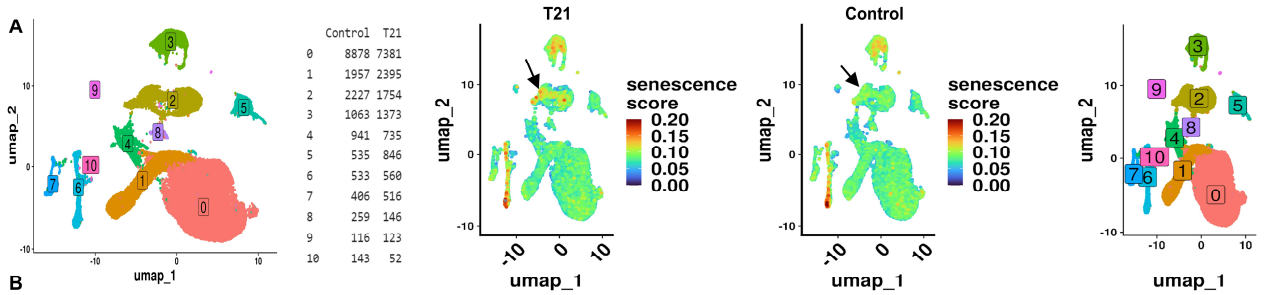


Figure 2. Reduced pulmonary vascular development in trisomy 21 lungs. (**A**) Representative immunofluorescence staining for von Willebrand factor (vWF, green) and CD31 (red) in euploid and T21 fetal lungs at 12–13 and 16–17 weeks gestation. Nuclei were counterstained with DAPI (blue). Arrows denote vWF or CD31 positive cells. (**B**) Quantification of vWF-positive vessels and CD31-positive endothelial cells in euploid and T21 lungs. Scale bars = 50 μm. Data are presented as mean ± SEM. n = 4 lungs/group. * $p < 0.05$ and ** $p < 0.01$ versus euploid controls.

3.3. Single-Cell Transcriptomic Analysis Identifies Epithelial Cells as the Primary Senescent Population

To identify the cellular origin of senescence within the fetal lung, publicly available human fetal lung single-cell RNA sequencing datasets (GSE272470) were reanalyzed. Unsupervised clustering identified multiple epithelial, endothelial, mesenchymal, and immune cell populations (Figure 3A, left panel). Senescence scores in cluster 2 were apparent in T21 compared to control (Figure 3A, middle panel). Cell-type annotation demonstrated that cluster 2 consisted predominantly of bronchiolar and alveolar epithelial cells (>98%) (Figure 3B). Because epithelial cells exhibited the strongest senescence-associated transcriptional signature, subsequent analyses focused on this epithelial compartment.



B

Cell type or status	Cluster										
	0	1	2	3	4	5	6	7	8	9	10
FETAL_LUNG_BRONCHIOLAR_AND_ALVEOLAR_EPITHELIAL_CELLS	49	24	3607	5	122	12	3	4	27	1	0
FETAL_LUNG_CILIATED_EPITHELIAL_CELLS	1	0	11	0	1	0	0	0	1	159	0
FETAL_LUNG_CSH1_CSH2_POSITIVE_CELLS	225	353	12	9	180	100	1	1	10	0	0
FETAL_LUNG_LYMPHATIC_ENDOTHELIAL_CELLS	9	8	1	184	9	3	0	0	1	0	0
FETAL_LUNG_LYMPHOID_CELLS	3	1	0	0	38	1	1	908	4	0	136
FETAL_LUNG_MEGAKARYOCYTES	20	356	1	1	76	185	1	1	109	1	3
FETAL_LUNG_MESOTHELIAL_CELLS	183	219	3	2	20	346	0	0	3	35	0
FETAL_LUNG_MYELOID_CELLS	5	2	4	1	31	1	1080	1	4	0	55
FETAL_LUNG_NEUROENDOCRINE_CELLS	2	4	3	0	1	12	0	0	1	40	0
FETAL_LUNG_SQUAMOUS_EPITHELIAL_CELLS	173	467	295	14	177	249	2	0	22	1	1
FETAL_LUNG_STROMAL_CELLS	15,542	2795	33	10	976	194	4	7	188	1	0
FETAL_LUNG_VASCULAR_ENDOTHELIAL_CELLS	47	122	11	2210	44	272	1	0	34	0	0
FETAL_LUNG_VISCERAL_NEURONS	0	1	0	0	1	6	0	0	1	1	0

Cluster 2: >98% cells are epithelial cells

Figure 3. Single-cell transcriptomic analysis identifies epithelial populations and senescence signatures in human fetal lungs. (**A**) Uniform Manifold Approximation and Projection (UMAP) plots showing major cell clusters identified by single-cell RNA sequencing of euploid control and T21 fetal lungs, with cell numbers in each cluster indicated for each group. Senescence scores are overlaid on UMAP plots to show their distribution across cell populations. Arrows indicate regions with higher senescence scores. (**B**) Cell-type annotation of major clusters based on established lineage-specific markers, showing that epithelial cells are predominantly represented in cluster 2.

3.4. Subclustering Identifies Type I Alveolar Cells and Club Cells as Major Senescent Epithelial Populations

To further characterize epithelial heterogeneity, cluster 2 cells were subjected to secondary clustering analysis. This analysis identified multiple epithelial subpopulations corresponding to type II alveolar cells, type I alveolar cells, transitional epithelial cells, Club cells, and epithelial cells displaying mesenchymal features (Figure 4A). The distribution of individual epithelial subclusters among the major epithelial populations is shown in Figure 4B.

A

Subcluster	Clusters										
	0	1	2	3	4	5	6	7	8	9	10
0	3722	0	0	0	0	0	0	0	0	0	0
1	2511	233	0	0	0	0	0	0	0	0	0
2	2365	0	0	0	0	0	0	0	0	0	0
3	2096	0	0	0	0	0	0	0	0	0	0
4	1926	0	0	0	0	0	0	0	0	0	0
5	0	0	1854	0	0	0	0	0	0	0	0
6	0	0	0	1648	0	0	0	0	0	0	0
7	0	1621	0	0	0	0	0	0	0	0	0
8	1584	0	0	0	0	0	0	0	0	0	0
9	5	0	0	0	0	1380	0	0	0	0	0
10	0	1297	0	0	0	0	0	0	0	0	0
11	0	0	1224	0	0	0	0	0	0	0	0
12	0	1197	0	0	0	0	0	0	0	0	0
13	0	0	45	0	976	0	0	0	0	0	0
14	343	1	0	0	593	0	0	0	0	0	0
15	693	1	1	0	0	1	0	0	0	0	0
16	0	0	0	0	0	0	0	669	0	0	0
17	624	1	1	1	0	0	0	0	2	0	0
18	0	0	0	623	0	0	0	0	0	0	0
19	0	0	0	0	0	0	557	0	0	0	0
20	0	0	0	0	0	0	535	0	0	0	0
21	0	0	441	0	0	0	0	0	0	0	0
22	9	1	415	0	0	0	0	0	0	0	0
23	6	0	0	0	0	0	0	0	402	0	0
24	375	0	0	0	0	0	0	0	0	0	0
25	0	0	0	0	106	0	1	0	1	0	195
26	0	0	0	0	1	0	0	253	0	0	0
27	0	0	0	0	0	0	0	0	0	204	0
28	0	0	0	164	0	0	0	0	0	0	0
29	0	0	0	0	0	0	0	0	0	35	0

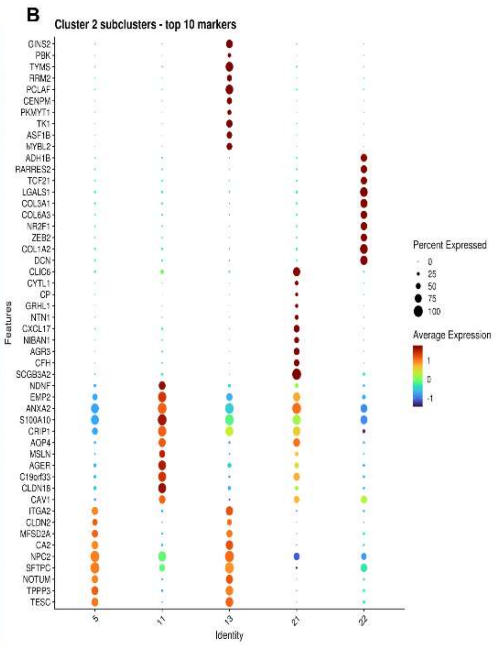
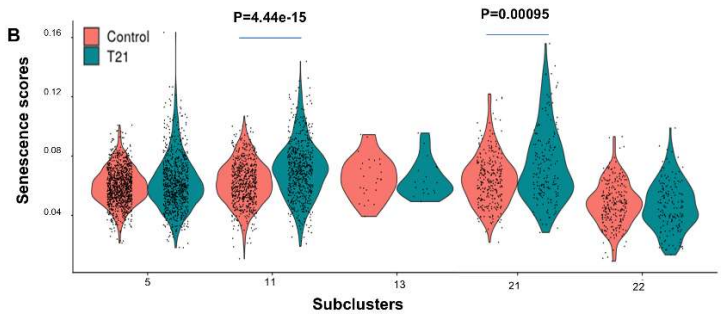


Figure 4. Subclustering analysis identifies distinct epithelial cell populations in human fetal lungs. (**A**) Distribution of subclusters generated by subclustering analysis across the original single-cell clusters. Epithelial cells from cluster 2 were resolved into five major subclusters, including subclusters 5, 11, 13, 21, and 22. (**B**) Dot plot showing the top marker genes for these epithelial subclusters. Dot size represents the percentage of cells expressing each gene, and color indicates average expression. Distinct marker-gene profiles were used to characterize the epithelial subpopulations.

Marker gene analysis identified subcluster 5 as type II alveolar cells, subcluster 11 as type I alveolar cells, subcluster 13 as proliferative transitional epithelial cells, subcluster 21 as Club cells, and subcluster 22 as epithelial cells exhibiting mesenchymal characteristics (Figure 5A). Calculation of senescence scores demonstrated significantly increased senescence signatures in type I alveolar cells (subcluster 11) and Club cells (subcluster 21) in T21 lungs compared with euploid controls (Figure 5B). These findings suggest that senescence occurs preferentially within specific epithelial populations rather than uniformly across the lung epithelium.

A

Subcluster	Top marker genes	Cell type or status
Subcluster 5	SFTPC, MFSD2A.	Type 2 cells
Subcluster 11	AGER, EMP2, CLDN18; express SFTPC at a low level.	Type 1 cells
Subcluster 13	Highly express GINS2, PCLAF, TYMS, RRM2, TK1. Express SFTPC CLADN2, EMP2, S100A10, ANAX2, and AGER at a medium or low level.	Type 2 differentiation into type 1, with highly proliferative
Subcluster 21	SCGB3A2, CYTL1, AGR3.	Clara/Club cells
Subcluster 22	Highly express COL1A2, COL3A1, COL6A3 and ZEB2. Also express SFTPC and CLADN2 at a low level.	Epithelial-to-mesenchymal transition



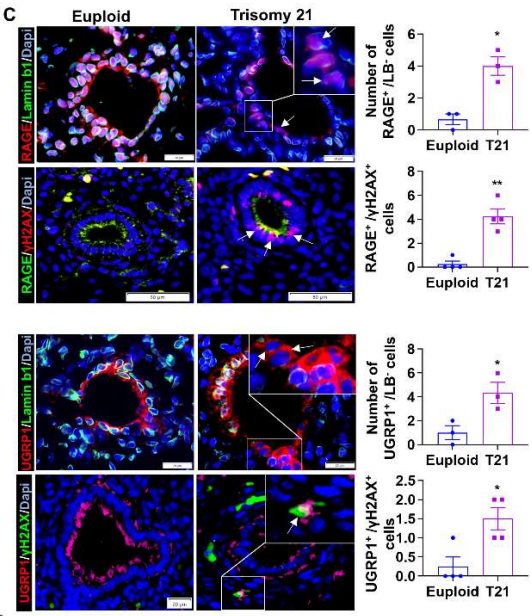


Figure 5. Type I alveolar cells and Club cells exhibit increased senescence signatures in trisomy 21 fetal lungs. (**A**) Epithelial subclusters identified by single-cell transcriptomic analysis and their representative marker genes and cell-type annotations. (**B**)

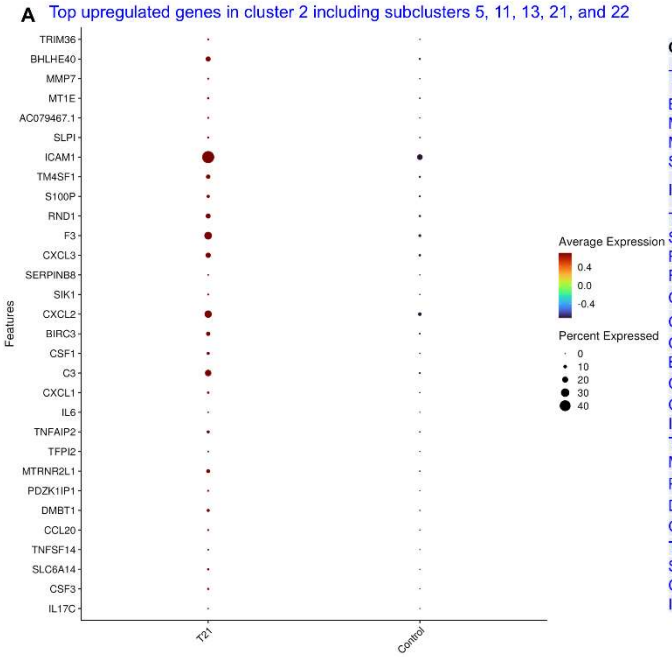
Senescence scores across epithelial subclusters in euploid control and T21 fetal lungs. Senescence scores were significantly increased in type I alveolar cells (subcluster 11) and Club cells (subcluster 21) in T21 lungs. (**C**) Representative immunofluorescence staining and quantification of $RAGE^+$/lamin $b1^-$ and $RAGE^+/\gamma H2AX^+$ type I alveolar cells and $UGRP1^+$/lamin $b1^-$ Club cells in euploid and T21 fetal lungs. Arrows indicate double-positive cells. Scale bars, 25 μm or 50 μm. Data are presented as mean ± SEM. $n = 4$ lungs/group. * $p < 0.05$, ** $p < 0.01$.

3.5. Immunofluorescence Validation Confirms Senescence in Type I Alveolar Cells and Club Cells

To validate the transcriptomic findings in tissue sections, dual immunofluorescence staining was performed using lamin b1 and γH2AX as senescence indicators together with cell-type-specific markers. Type I alveolar cells were identified by RAGE expression, whereas Club cells were identified by UGRP1 expression (Figure 5C). T21 lungs exhibited significantly increased numbers of RAGE-positive cells lacking lamin b1 compared with euploid controls. Furthermore, numbers of co-localization of RAGE with γH2AX was increased in T21 lungs, indicating enhanced senescence within type I alveolar cells (Figure 5C). Similarly, $UGRP1^+$ Club cells exhibited significantly increased γH2AX positivity and loss of lamin b1 in T21 lungs (Figure 5C). These findings confirm that type I alveolar cells and Club cells are major senescent epithelial populations in the developing T21 lung.

3.6. Senescence-Associated Inflammatory Programs Are Activated in Trisomy 21 Epithelial Cells

Differential gene expression analysis revealed widespread activation of inflammatory and stress-response pathways in T21 epithelial cells. Several genes associated with senescence-associated secretory phenotype signaling, including CXCL1, CXCL2, CXCL3, IL6, ICAM1, C3, CSF1, and TNFAIP2, were significantly upregulated in T21 epithelial populations (Figure 6A). Functional annotation demonstrated enrichment of pathways involved in inflammation, extracellular matrix remodeling, cytokine signaling, and immune cell recruitment (Figure 6B). These findings indicate activation of a pro-inflammatory senescence-associated transcriptional program in T21 epithelial cells.



B

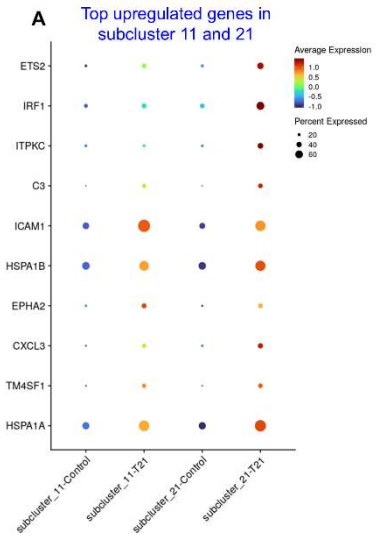
Gene	Function
TRIM36	Microtubular protein; E3 ubiquitin ligase; crucial for early development; inhibits cell cycle
BHLHE40	Circadian gene involved in organ development and senescence; regulates p21
MMP7	Matrix metalloproteinase-7; ECM remodeling, inflammation, tissue repair
MT1E	Metallothionein 1E; tumor suppressor; increases life span
SLP1	Secreted inhibitor protecting epithelial tissues from serine proteases
ICAM1	Mediating leukocyte–endothelial interactions; inflammation; senescence-linked regulation
TM4SF1	Surface protein; nanopodia formation; migration; endothelial progenitors
S100P	Calcium-binding protein
RND1	Rho GTPase family; inhibits cell cycle
F3	Coagulation Factor III
CXCL1	SASP chemokine reinforcing senescence
CXCL2	SASP chemokine involved in inflammatory signaling
CXCL3	SASP chemokine, inflammation mediator
BIRC3	Anti-apoptotic IAP protein binding TRAF1/2
CSF1	Macrophage regulator; SASP factor
C3	Complement component; increased in aging
IL6	Major SASP cytokine driving inflammatory senescence
TNFAIP2	TNF-α-induced protein; pulmonary differentiation; elevated in Down Syndrome
MTRNR2L1	Pseudogene related to mitochondrial 16S
PDZK1IP1	MAP17; increased in senescence; upregulates IL-6
DMBT1	Interacts with SP-D; alters surfactant structure
CCL20	Chemokine; SASP-associated immune recruitment
TNFSF14	LIGHT; attenuates neovascularization
SLC6A14	Amino acid transporter; CF secretion defect modifier
CSF3	Associated with Down Syndrome
IL17C	Associated with Down Syndrome

Figure 6. Senescence-associated inflammatory genes are increased in trisomy 21 epithelial cells. (**A**) Dot plot showing representative genes significantly upregulated in T21 epithelial cells compared with euploid controls across epithelial subclusters 5, 11, 13, 21, and 22. Dot size represents the percentage of cells expressing each gene, and color indicates average expression. Upregulated genes include inflammatory and senescence-associated mediators, including ICAM1, CXCL1, CXCL2, CXCL3, C3, IL6, and CCL20, as well as genes involved in cellular stress and cell-cycle regulation. (**B**) Functional annotation of

representative upregulated genes highlighting their roles in inflammatory signaling, cellular stress responses, and senescence-associated pathways.

3.7. Type I Alveolar Cells and Club Cells Display Overlapping Senescence-Associated Transcriptional Signatures

To further define epithelial cell-specific responses, we examined differentially expressed genes in type I alveolar cells and Club cells. Type I alveolar cells showed increased expression of ICAM1, HSPA1A, HSPA1B, EPHA2, and TM4SF1, consistent with enhanced cellular stress, proteostasis, and inflammatory signaling. In contrast, Club cells exhibited prominent upregulation of ETS2, IRF1, ITPKC, C3, and CXCL3, indicative of interferon, complement, and inflammatory/SASP-associated signaling (Figure 7A,B). These findings demonstrate both shared and distinct senescence-associated transcriptional responses in the fetal lung epithelium.



B

Gene	Function
EST2	Enables telomeric DNA binding activity.
IRF1	Interferon regulatory factor 1; involved in alveolar growth arrest.
ITPKC	Regulates Ca2+/NFAT signaling.
C3	Complement signaling.
ICAM1	Facilitates inflammatory cell migration.
HSPA1B	Encodes Hsp70-2; maintains proteostasis.
EPHA2	Receptor tyrosine kinase; SASP-associated.
CXCL3	Chemokine; SASP inflammatory mediator.
TM4SF1	Surface membrane antigen; endothelial/stem cell marker.
HSPA1A	Encodes Hsp70; maintains proteostasis.

Figure 7. Type I alveolar cells and Club cells exhibit cell-specific transcriptional responses in trisomy 21 fetal lungs. (**A**) Dot plot showing representative genes upregulated in type I alveolar cells (subcluster 11) and Club cells (subcluster 21) from T21 fetal lungs compared with their respective euploid controls. Dot size represents the percentage of cells expressing each gene, and color indicates average expression. (**B**) Functional annotation of representative upregulated genes and their roles in inflammatory signaling, cellular stress, proteostasis, and senescence-associated pathways.

3.8. Developmental Regulators Are Suppressed in Trisomy 21 Epithelial Cells

Analysis of downregulated genes in T21 epithelial cells revealed suppression of multiple programs involved in epithelial differentiation, extracellular matrix organization, angiogenesis, and tissue maturation (Supplementary Figure S1A,B). Furthermore, genes associated with chromatin remodeling (SMARCA5), extracellular matrix and angiogenic signaling (CCN1), metabolism (UCP2 and FABP5), Notch/Wnt signaling (JAG1, NOTCH3, and DACT2), and transcriptional control of lung development and epithelial identity (PBX1, GRHL2, SHH, CEBPA, and NKX2-1) were reduced in T21 cells (Supplementary Figure S2A,B). These findings indicate that the senescence-associated transcriptional phenotype in T21 fetal lung epithelial cells coincides with attenuation of developmental programs required for epithelial differentiation and lung morphogenesis.

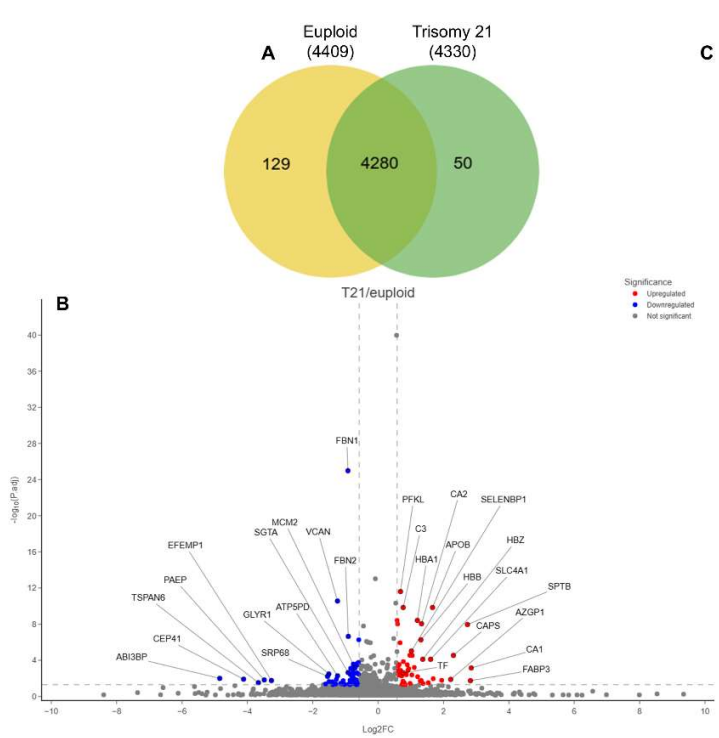
3.9. Functional Enrichment Analyses Reveal Inflammatory Activation and Suppression of Developmental Programs in T21 Fetal Lungs

To define the biological processes altered in T21 lungs, Gene Ontology (GO) and KEGG pathway enrichment analyses were performed. Upregulated genes were enriched for innate and adaptive immune

responses, cytokine and chemokine signaling, MAPK and NF-κB signaling, Toll-like and NOD-like receptor pathways, and cytosolic DNA sensing (Supplementary Figure S3). In contrast, downregulated genes were enriched in processes related to cell differentiation, epithelial cell proliferation, developmental regulation, and DNA methylation (Supplementary Figure S4). Together, these findings indicate a transcriptional shift toward inflammatory and stress-responsive signaling accompanied by suppression of developmental and proliferative programs in T21 fetal lungs.

3.10. Proteomic Profiling Reveals Broad Molecular Alterations in T21 Fetal Lungs

To independently assess molecular alterations associated with T21, quantitative proteomic profiling was performed in euploid and T21 fetal lungs. Among 4409 proteins detected in euploid lungs and 4330 proteins detected in T21 lungs, 4280 were shared between groups, whereas 129 and 50 proteins were uniquely detected in euploid and T21 lungs, respectively (Figure 8A). Differential protein abundance analysis further revealed marked alterations in proteins involved in extracellular matrix organization, cell proliferation, metabolism, and immune regulation (Figure 8B,C). For instance, FBN1, FBN2, MCM2, VCAN, EFEMP1, and ATP5PD were reduced, whereas C3, PFKL, CA2, APOB, and AZGP1 were increased in T21 fetal lungs, suggesting broad alterations in structural, proliferative, metabolic, and inflammatory processes.



C

Gene Symbol	Core Function
FBN1	Fibrillin-1. Major component of the extracellular matrix (ECM) microfibrils; provides strength and elasticity to lung parenchyma and blood vessel walls.
FBN2	Fibrillin-2. Component of the ECM microfibrils; involved in elastogenesis and essential for proper tissue development and patterning (like lung branching).
MCM2	Part of the replication licensing complex; essential for initiating DNA replication and cell cycle progression (i.e., cell proliferation).
VCAN	Versican. A large proteoglycan in the ECM; involved in cell adhesion, migration, and proliferation, contributing to tissue structure and inflammation.
SGTA	Involved in protein quality control and trafficking; helps target proteins to the endoplasmic reticulum.
GLYR1	A ligand-gated ion channel; important for inhibitory neurotransmission, though its function in the lung is complex (potentially related to ion transport).
ATP5PD	A component of the mitochondrial ATP synthase complex (Complex V); essential for cellular energy production (ATP synthesis).
SRP68	Signal Recognition Particle 68. Mmediates the targeting of secreted and membrane proteins to the endoplasmic reticulum.
EFEMP1	An ECM glycoprotein that promotes cell proliferation and migration and is involved in tissue repair and remodeling.
PFKL	Phosphofructokinase, Liver Type. A key regulatory enzyme in glycolysis; catalyzes the committed step of breaking down glucose for energy.
CA2	Carbonic Anhydrase 2. Catalyzes the interconversion of carbon dioxide and water to bicarbonate and protons; crucial for pH balance and CO_2 transport.
C3	Complement Component 3. Central protein of the complement system; plays a key role in innate immunity and inflammation.
APOB	Apolipoprotein B. The primary structural protein of low-density lipoproteins (LDL); involved in lipid transport and metabolism.
HBA1	Hemoglobin Subunit Alpha 1. Component of the hemoglobin tetramer (HBA1/HBB); essential for oxygen transport.
HBB	Hemoglobin Subunit Beta. Component of the hemoglobin tetramer (HBA1/HBB); essential for oxygen transport.
SLC4A1	A bicarbonate/chloride exchanger protein for maintaining cell volume and pH homeostasis.
HBZ	Hemoglobin Subunit Zeta. Component of embryonic hemoglobin; reflects the presence of less mature, fetal-type red blood cells.
AZGP1	Alpha-2-Glycoprotein 1, Zinc-Binding. Secreted protein involved in lipid metabolism, cell proliferation, and differentiation.
CAPS	Calcyphosin. Involved in calcium signaling; plays a role in regulating secretion and cellular responses.
SPTB	A cytoskeletal protein important for maintaining cell shape, stability, and membrane organization.

Figure 8. Proteomic profiling reveals differential protein abundance in trisomy 21 fetal lungs. (**A**) Venn diagram showing proteins detected by quantitative proteomic analysis of euploid and T21 fetal lungs. A total of 4280 proteins were shared between groups, whereas 129 proteins were detected only in euploid lungs and 50 only in T21 lungs. (**B**) Volcano plot showing differentially abundant proteins in T21 versus euploid fetal lungs. Red and blue indicate proteins significantly increased and decreased, respectively, in T21 lungs; gray indicates proteins with no significant differences. Selected differentially abundant proteins are labeled. (**C**) Functional annotation of representative differentially abundant proteins, including proteins involved in extracellular matrix organization, cell proliferation, mitochondrial energy metabolism, glycolysis, complement signaling, lipid metabolism, and cellular homeostasis.

3.11. T21 Fetal Lungs Exhibit Inflammatory and Metabolic Reprogramming with Suppression of Proliferative and Genome-Maintenance Pathways

KEGG pathway analysis revealed that proteins increased in T21 lungs were enriched in complement and coagulation cascades, ECM-receptor interaction, PPAR and adipocytokine signaling, focal adhesion, glycolysis/gluconeogenesis, and the pentose phosphate pathway (Figure 9). Consistent with these findings, Gene Ontology analysis demonstrated enrichment of complement activation, humoral immune responses, extracellular matrix organization, lipid metabolic processes, glycolytic processes, and cellular oxidant detoxification (Figure 10). In contrast, proteins reduced in T21 lungs were enriched in pathways related to cell cycle, DNA replication, mismatch repair, ribosome and spliceosome function, and antigen processing and presentation (Supplementary Figure S5). GO analysis further demonstrated suppression of DNA repair and DNA metabolic processes, TGF-β receptor signaling, and other cellular regulatory programs (Supplementary Figure S6). Together, these findings indicate a shift toward inflammatory, metabolic, and stress-responsive pathways accompanied by attenuation of proliferative and genome-maintenance programs in T21 fetal lungs.

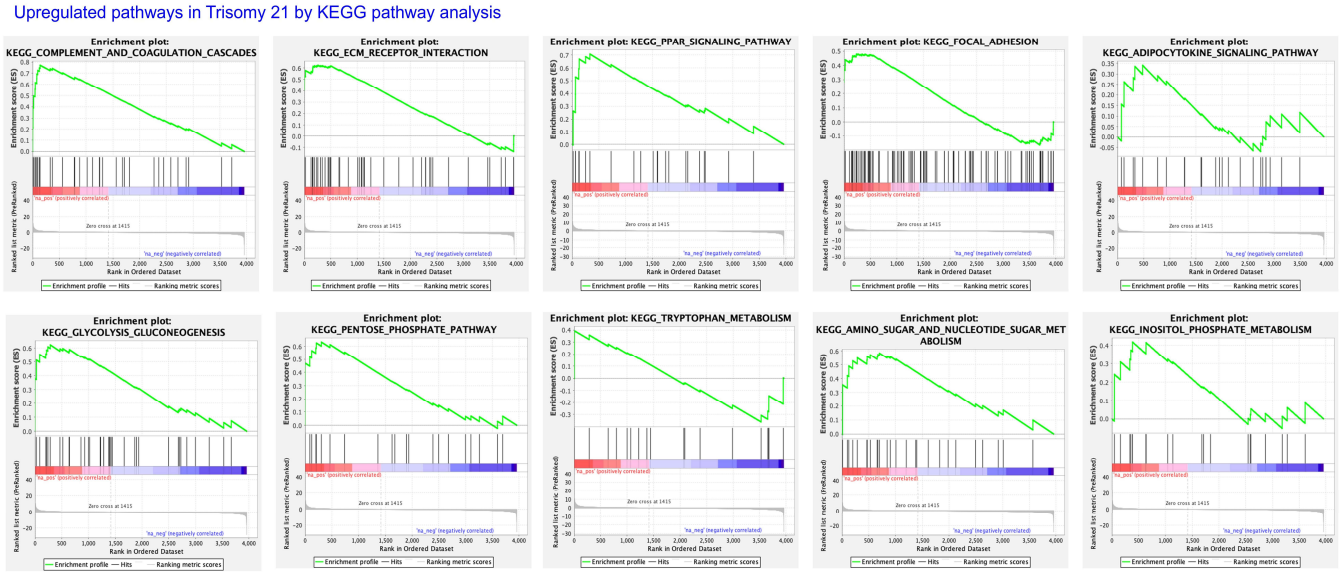


Figure 9. Proteomic pathway analysis reveals enrichment of inflammatory, extracellular matrix, and metabolic pathways in trisomy 21 fetal lungs. Gene set enrichment analysis of proteins increased in T21 fetal lungs compared with euploid controls using KEGG pathways. Enriched pathways include complement and coagulation cascades, ECM-receptor interaction, PPAR signaling, focal adhesion, adipocytokine signaling, glycolysis/gluconeogenesis, pentose phosphate pathway, tryptophan metabolism, amino sugar and nucleotide sugar metabolism, and inositol phosphate metabolism.

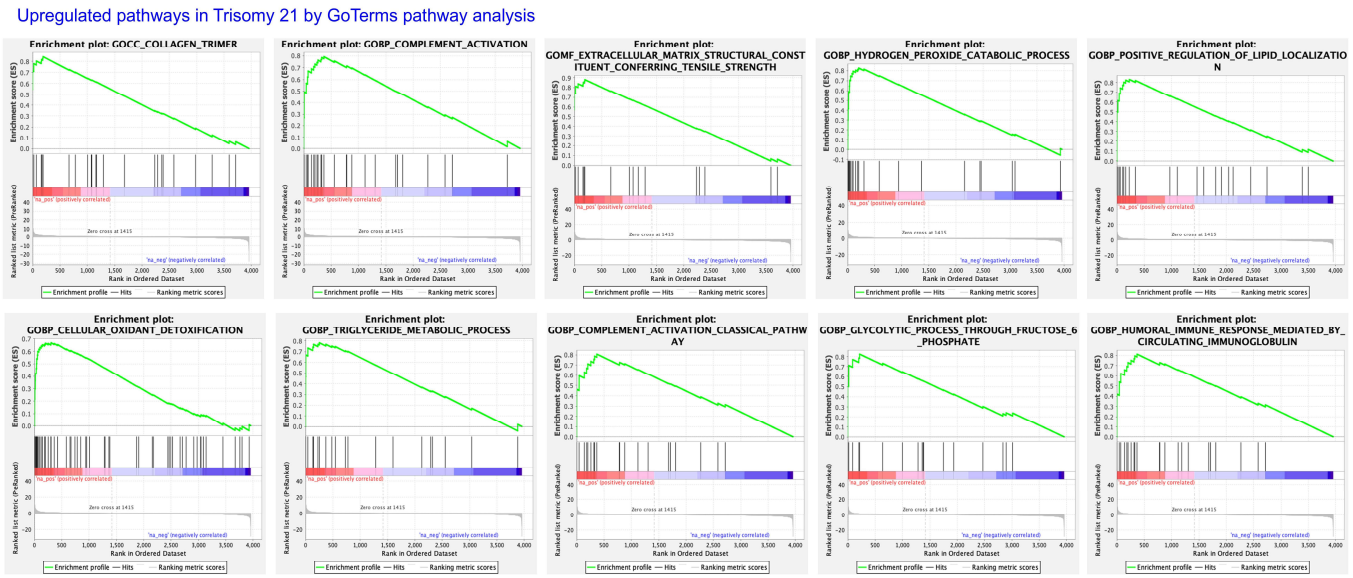


Figure 10. Proteomic Gene Ontology analysis reveals enrichment of immune, extracellular matrix, metabolic, and oxidative stress-related processes in trisomy 21 fetal lungs. Gene set enrichment analysis of proteins increased in T21 fetal lungs compared with euploid controls using Gene Ontology (GO) terms. Enriched processes include collagen trimer and extracellular matrix structural organization, complement activation and humoral immune responses, hydrogen peroxide catabolism and cellular oxidant detoxification, lipid localization and triglyceride metabolism, and glycolytic processes.

3.12. T21-Specific Proteins Are Associated with Inflammatory, Metabolic, and Cellular Stress Responses

Analysis of proteins uniquely detected in each group further distinguished the T21 proteomic phenotype. Proteins detected only in euploid lungs included EMILIN2, TIMP3, ADAMTSL4, SCARA5, ENPP1, EGLN1, RRM2, ANAPC5, BRD7, and RBM19, which are associated with extracellular matrix remodeling, angiogenesis and vascular-epithelial coupling, developmental plasticity, cell proliferation, and transcriptional regulation (Supplementary Table S2). In contrast, proteins uniquely detected in T21 lungs included MORC3, ZMYND11, PTPN13, KRAS, PGLYRP2, C9, C8A, LRG1, ADAM17, IFI35, CYB5B, DHRS11, NAGLU, TOM1L2, ANXA8, and CASTOR1, implicating genome-stress responses, innate immune and complement signaling, redox and metabolic stress, proteostasis, and altered cellular architecture (Supplementary Table S3). These proteomic alterations complement the transcriptomic findings and support a T21 fetal lung phenotype characterized by heightened inflammatory and stress-associated signaling, metabolic reprogramming, and attenuation of proliferative and developmental programs, collectively consistent with a senescence-associated molecular state.

4. Discussion

This study identifies cell-specific epithelial senescence as a prominent feature of the developing human T21 lung. The principal advance is the localization of senescence-associated signatures to specific epithelial populations, particularly type I alveolar and Club cells, rather than a uniform increase across the lung. These findings are supported by single-cell transcriptomic analysis and immunofluorescence demonstrating increased γH2AX positivity and loss of lamin b1 in RAGE-positive and UGRP1-positive epithelial populations. The changes are accompanied by abnormal lung architecture, reduced pulmonary vascularization, increased inflammatory signaling, and altered developmental and metabolic programs. Together, these findings suggest that epithelial senescence may contribute to impaired lung development in T21.

Our findings extend prior studies showing increased senescence markers in T21 tissues and developing T21 lungs [4,15,16]. Down syndrome is increasingly recognized as a condition associated with accelerated biological aging, including oxidative stress, genomic instability, and mitochondrial dysfunction, all of

which can promote cellular senescence [8–13,24,25]. The senescence-associated changes observed in fetal T21 lungs may reflect premature activation of aging-related pathways and/or chromosome dosage-induced developmental stress. Although these processes share molecular features, their relative contributions remain unclear. Nevertheless, our findings suggest that senescence-associated pathways are activated during critical stages of fetal lung development.

The preferential involvement of type I alveolar and Club cells may reflect differences in differentiation status, developmental stage, metabolic demands, and susceptibility to cellular stress. Type I alveolar cells contribute to epithelial-endothelial communication, whereas Club cells have important roles in airway maintenance and repair [26,27]. Senescence in these populations may therefore disrupt lung development and potentially compromise postnatal airway regeneration, increasing susceptibility to respiratory complications in Down syndrome. The less pronounced senescence signatures in type II alveolar cells suggest cell-specific responses to chromosome dosage imbalance. Furthermore, fetal epithelial cells may exhibit transitional differentiation states, and RAGE expression alone does not exclude co-expression of type II alveolar or Club cell markers [27]. The reduced pulmonary vascularization observed in T21 lungs may result from direct effects of T21 on endothelial cells, altered epithelial-endothelial communication, or both. Disruption of epithelial-derived angiogenic signals, potentially involving VEGF and SHH pathways [27], may contribute to impaired vascular development, although these mechanisms remain to be established.

A second major finding is the convergence of transcriptomic and proteomic evidence supporting inflammatory and stress-associated responses. T21 epithelial cells exhibited increased expression of SASP-associated genes, including IL6, CXCL1, CXCL2, CXCL3, ICAM1, and C3. Whole-lung proteomic analysis further demonstrated enrichment of complement and immune-related pathways. These findings suggest that senescent epithelial cells may influence the surrounding microenvironment through inflammatory and paracrine signaling. However, whether these mediators are specifically secreted by senescent epithelial cells remains unknown. Increased interferon signaling and immune dysregulation are recognized features of T21 [28,29], and endothelial interferon responses have been implicated in pulmonary vascular abnormalities [30]. Thus, epithelial senescence, immune activation, and endothelial dysfunction may be interconnected processes that contribute to abnormal lung development.

The suppression of developmental and proliferative programs provides another potential link between senescence and impaired morphogenesis. Rather than reflecting accelerated epithelial maturation, these changes may indicate altered differentiation associated with cellular stress and reduced developmental competence [31]. ECM remodeling may further contribute to abnormal lung architecture. Our proteomic findings revealed alterations in ECM-associated proteins and pathways, suggesting disruption of the extracellular environment. Senescent epithelial cells may influence ECM organization through SASP-associated signaling [32], while direct effects of chromosome dosage imbalance on mesenchymal cells may also contribute. Such changes could disrupt epithelial-mesenchymal interactions, epithelial differentiation, and branching morphogenesis [33]. However, fibroblast activation and senescence-driven ECM remodeling were not directly demonstrated.

The proteomic findings provide additional support for a shift from proliferative and genome-maintenance programs toward inflammatory, metabolic, ECM-related, and stress-responsive pathways in T21 fetal lungs. These alterations complement the transcriptomic findings and suggest broader dysregulation of developmental processes. However, because proteomic analyses were performed on whole-lung tissues, the contributions of individual cell populations and the mechanisms underlying these changes remain to be determined.

Developmental senescence is a physiological process contributing to embryonic tissue remodeling and organogenesis [34–36]. In T21 lungs, chromosome dosage imbalance may enhance or dysregulate this process through increased cellular stress, potentially disrupting normal epithelial differentiation and tissue development. However, epithelial senescence could represent either a contributor to abnormal

morphogenesis or a secondary response to developmental abnormalities. These mechanisms are not mutually exclusive, as senescence-associated inflammatory signaling may amplify existing developmental defects. The temporal relationship between senescence and structural abnormalities, as well as the persistence of these changes after birth, remains unknown.

Several limitations should be acknowledged. Human fetal lung samples were limited, restricting assessment of gestational age- and sex-dependent effects. The cross-sectional design precludes determination of causal and temporal relationships between epithelial senescence and impaired lung development. Although senescence-associated transcriptional signatures, γH2AX positivity, and loss of lamin b1 provide complementary evidence of epithelial senescence, additional markers, including p16, p21, and Ki67, were not evaluated. Furthermore, SASP protein secretion by senescent epithelial cells, co-expression of additional epithelial lineage markers, and the functional contributions of epithelial senescence to vascular and ECM abnormalities were not directly assessed. Nevertheless, our integrated findings identify cell-specific epithelial senescence-associated changes as an important feature of impaired fetal lung development in T21.

5. Conclusions

This study identifies cell-specific epithelial senescence as a prominent feature of the developing human T21 lung, with preferential involvement of type I alveolar and Club cells. The senescence phenotype is associated with inflammatory and stress-responsive signaling, suppression of developmental and genome-maintenance programs, and abnormal pulmonary morphogenesis and vascular development. These findings suggest that epithelial senescence may represent an important component of developmental dysregulation in T21 and provide a rationale for future mechanistic studies to determine whether senescence contributes directly to impaired lung development.

Supplementary Materials

The following supporting information can be found at: https://www.sciepublish.com/article/pii/1322, Figure S1. Developmental and epithelial regulatory genes are reduced in trisomy 21 fetal lung epithelial cells. Figure S2. Key developmental and homeostatic programs are suppressed in type I alveolar and Club cells in trisomy 21 fetal lungs. Figure S3. Upregulated genes in trisomy 21 fetal lungs are enriched in inflammatory and immune signaling pathways. Figure S4. Downregulated genes in trisomy 21 fetal lungs are enriched in developmental, differentiation, and epigenetic regulatory processes. Figure S5. Proteomic KEGG pathway analysis reveals suppression of cell proliferation, DNA replication and repair, and protein processing pathways in trisomy 21 fetal lungs. Figure S6. Proteomic Gene Ontology analysis reveals suppression of DNA repair, protein processing, and developmental regulatory pathways in trisomy 21 fetal lungs. Table S1. Antibodies used in this study. Table S2. Proteins expressed only in the euploid group. Table S3. Proteins expressed only in the trisomy 21 group.

Statement of the Use of Generative AI and AI-Assisted Technologies in the Writing Process

During the preparation of this manuscript, the authors used ChatGPT (OpenAI) to assist with language editing, grammar correction, and improving the clarity and readability of the manuscript. After using this tool, the authors reviewed and edited the content as needed and take full responsibility for the content of the published article.

Acknowledgments

We thank the Brown University Proteomics Core Facility for performing proteomics analyses and the Ocean State Research Institute/Providence VA Medical Center Cell Isolation and Organ Function Core Facility (RRID: SCR_028797) for performing immunofluorescence.

Author Contributions

E.K. and G.H. performed immunostaining, J.W. performed scRNA-seq reanalysis, I.A.G. collected and provided human lung tissues, A.U. performed data analysis of proteomics, P.A.D. assisted with the experimental design and revised the manuscript, H.Y. designed the study, acquired and analyzed data, drafted the initial manuscript, and revised the manuscript.

Ethics Statement

The study was conducted in accordance with the principles of the Declaration of Helsinki. Human fetal lung tissues were obtained from the Birth Defects Research Laboratory (BDRL) at the University of Washington under a protocol approved by the University of Washington Institutional Review Board (IRB No. STUDY00000380, 7/9/2024). All tissues were de-identified and used for research purposes in accordance with applicable institutional and ethical guidelines.

Informed Consent Statement

Written informed consent was obtained from all pregnant donors prior to fetal tissue donation.

Data Availability Statement

The data supporting the findings of this study are available within the article and its Supplementary Materials. Additional data are available from the corresponding author upon reasonable request.

Funding

This research was supported in part by the National Institutes of Health grant R01HL166327 (H.Y.), R24HD000836 (I.A.G.), an Institutional Development Award (IDeA) from the National Institute of General Medical Sciences of the National Institutes of Health under grant P30GM149398 (H.Y. and P.A.D.), and the Warren Alpert Foundation of Brown University (P.A.D.).

Declaration of Competing Interest

The authors declare that they have no known competing financial interests or personal relationships that could have appeared to influence the work reported in this paper.

References

1. Tsou AY, Bulova P, Capone G, Chicoine B, Gelaro B, Harville TO, et al. Medical Care of Adults with Down Syndrome: A Clinical Guideline. *JAMA* **2020**, *324*, 1543–1556. DOI:10.1001/jama.2020.17024
2. Bull MJ. Down Syndrome. *N. Engl. J. Med.* **2020**, *382*, 2344–2352. DOI:10.1056/nejmra1706537
3. Davidson MA. Primary care for children and adolescents with Down syndrome. *Pediatr. Clin. North Am.* **2008**, *55*, 1099–1111. DOI:10.1016/j.pcl.2008.07.001
4. Danopoulos S, Bhattacharya S, Deutsch G, Nih LR, Slaunwhite C, Mariani TJ, et al. Prenatal histological, cellular, and molecular anomalies in trisomy 21 lung. *J. Pathol.* **2021**, *255*, 41–51. DOI:10.1002/path.5735
5. Colvin KL, Yeager ME. What people with Down Syndrome can teach us about cardiopulmonary disease. *Eur. Respir. Rev.* **2017**, *26*, 160098. DOI:10.1183/16000617.0098-2016

6. Thase ME. Longevity and mortality in Down's syndrome. *J. Ment. Defic. Res.* **1982**, *26*, 177–192. DOI:10.1111/j.1365-2788.1982.tb00144.x
7. Zhi C, Shi X, Chen S, Cai Z, Jiang X. Single-cell transcriptome analysis reveals critical causative candidates for Down syndrome-related lung diseases. *J. Genet. Genomics* **2026**, *53*, 75–86. DOI:10.1016/j.jgg.2025.05.009
8. Patterson D, Cabelof DC. Down syndrome as a model of DNA polymerase beta haploinsufficiency and accelerated aging. *Mech. Ageing Dev.* **2012**, *133*, 133–137. DOI:10.1016/j.mad.2011.10.001
9. Ge F, Pan Q, Qin Y, Jia M, Ruan C, Wei X, et al. Single-Cell Analysis Identify Transcription Factor BACH1 as a Master Regulator Gene in Vascular Cells During Aging. *Front. Cell Dev. Biol.* **2021**, *9*, 786496. DOI:10.3389/fcell.2021.786496
10. Walton CC, Begelman D, Nguyen W, Andersen JK. Senescence as an Amyloid Cascade: The Amyloid Senescence Hypothesis. *Front. Cell. Neurosci.* **2020**, *14*, 129. DOI:10.3389/fncel.2020.00129
11. Anderson G, Mackay N, Gilroy K, Hay J, Borland G, McDonald A, et al. RUNX-mediated growth arrest and senescence are attenuated by diverse mechanisms in cells expressing RUNX1 fusion oncoproteins. *J. Cell. Biochem.* **2018**, *119*, 2750–2762. DOI:10.1002/jcb.26443
12. Bruintjes JJ, Henning RH, Douwenga W, van der Zee EA. Hippocampal cystathionine beta synthase in young and aged mice. *Neurosci. Lett.* **2014**, *563*, 135–139. DOI:10.1016/j.neulet.2014.01.049
13. Litovchick L, Florens LA, Swanson SK, Washburn MP, DeCaprio JA. DYRK1A protein kinase promotes quiescence and senescence through DREAM complex assembly. *Genes Dev.* **2011**, *25*, 801–813. DOI:10.1101/gad.2034211
14. Meharena HS, Marco A, Dileep V, Lockshin ER, Akatsu GY, Mullahoo J, et al. Down-syndrome-induced senescence disrupts the nuclear architecture of neural progenitors. *Cell Stem Cell* **2022**, *29*, 116–130.e7. DOI:10.1016/j.stem.2021.12.002
15. Chen Y, Xiao Y, Zhang Y, Wang R, Wang F, Gao H, et al. Single-cell landscape analysis reveals systematic senescence in mammalian Down syndrome. *Clin. Transl. Med.* **2023**, *13*, e1310. DOI:10.1002/ctm2.1310
16. Belgacemi R, Cherry C, Thompson M, Koloko Ngassie M, Rehan A, El Alam I, et al. Elevated Senescence Markers in Developing Trisomy 21 Human Lungs. *Am. J. Respir. Cell Mol. Biol.* **2025**, *73*, 251–263. DOI:10.1165/rcmb.2024-0361oc
17. Dennery PA, Yao H. Emerging role of cellular senescence in normal lung development and perinatal lung injury. *Chin. Med. J. Pulm. Crit. Care Med.* **2024**, *2*, 10–16. DOI:10.1016/j.pccm.2024.01.001
18. Schindelin J, Arganda-Carreras I, Frise E, Kaynig V, Longair M, Pietzsch T, et al. Fiji: An open-source platform for biological-image analysis. *Nat. Methods* **2012**, *9*, 676–682. DOI:10.1038/nmeth.2019
19. Lipsett J. Human fetal lung morphometry at autopsy with new modeling to quantitate structural maturity. *Pediatr. Pulmonol.* **2017**, *52*, 771–778. DOI:10.1002/ppul.23675
20. Hao Y, Stuart T, Kowalski MH, Choudhary S, Hoffman P, Hartman A, et al. Dictionary learning for integrative, multimodal and scalable single-cell analysis. *Nat. Biotechnol.* **2024**, *42*, 293–304. DOI:10.1038/s41587-023-01767-y
21. Hafemeister C, Satija R. Normalization and variance stabilization of single-cell RNA-seq data using regularized negative binomial regression. *Genome Biol.* **2019**, *20*, 296. DOI:10.1186/s13059-019-1874-1
22. Aibar S, Gonzalez-Blas CB, Moerman T, Huynh-Thu VA, Imrichova H, Hulselmans G, et al. SCENIC: Single-cell regulatory network inference and clustering. *Nat. Methods* **2017**, *14*, 1083–1086. DOI:10.1038/nmeth.4463
23. Xu S, Hu E, Cai Y, Xie Z, Luo X, Zhan L, et al. Using clusterProfiler to characterize multiomics data. *Nat. Protoc.* **2024**, *19*, 3292–3320. DOI:10.1038/s41596-024-01020-z
24. Franceschi C, Garagnani P, Gensous N, Bacalini MG, Conte M, Salvioli S. Accelerated bio-cognitive aging in Down syndrome: State of the art and possible deceleration strategies. *Aging Cell* **2019**, *18*, e12903. DOI:10.1111/acel.12903
25. Lopez-Otin C, Blasco MA, Partridge L, Serrano M, Kroemer G. Hallmarks of aging: An expanding universe. *Cell* **2023**, *186*, 243–278. DOI:10.1016/j.cell.2022.11.001
26. Rawlins EL, Okubo T, Xue Y, Brass DM, Auten RL, Hasegawa H, et al. The role of Scgb1a1+ Clara cells in the long-term maintenance and repair of lung airway, but not alveolar, epithelium. *Cell Stem Cell* **2009**, *4*, 525–534. DOI:10.1016/j.stem.2009.04.002
27. Hines EA, Sun X. Tissue crosstalk in lung development. *J. Cell. Biochem.* **2014**, *115*, 1469–1477. DOI:10.1002/jcb.24811
28. Jin M, Xu R, Wang L, Alam MM, Ma Z, Zhu S, et al. Type-I-interferon signaling drives microglial dysfunction and senescence in human iPSC models of Down syndrome and Alzheimer's disease. *Cell Stem Cell* **2022**, *29*, 1135–1153.e8. DOI:10.1016/j.stem.2022.06.007
29. Frauenpreis A, Bhattacharya S, Belgacemi R, Sokolskiy P, Deutsch G, Jendzjowsky N, et al. Alterations in Resident Immune Cells in Prenatal Trisomy 21 Lungs. *Cells* **2025**, *14*, 1866. DOI:10.3390/cells14231866
30. Chorvinsky E, Bhattacharya S, Bera BS, Welham A, Ismat K, Lawlor CM, et al. Down Syndrome Alters Type III IFN and Proinflammatory Airway Epithelial Responses to Respiratory Syncytial Virus Infection. *Am. J. Respir. Cell Mol. Biol.* **2025**, *73*, 951–964. DOI:10.1165/rcmb.2025-0068oc

31. Munoz-Espin D, Serrano M. Cellular senescence: From physiology to pathology. *Nat. Rev. Mol. Cell Biol.* **2014**, *15*, 482–496. DOI:10.1038/nrm3823
32. Shannon JM, Hyatt BA. Epithelial-mesenchymal interactions in the developing lung. *Annu. Rev. Physiol.* **2004**, *66*, 625–645. DOI:10.1146/annurev.physiol.66.032102.135749
33. Zhou Y, Horowitz JC, Naba A, Ambalavanan N, Atabai K, Balestrini J, et al. Extracellular matrix in lung development, homeostasis and disease. *Matrix Biol.* **2018**, *73*, 77–104. DOI:10.1016/j.matbio.2018.03.005
34. Munoz-Espin D, Canamero M, Maraver A, Gomez-Lopez G, Contreras J, Murillo-Cuesta S, et al. Programmed cell senescence during mammalian embryonic development. *Cell* **2013**, *155*, 1104–1118. DOI:10.1016/j.cell.2013.10.019
35. Storer M, Mas A, Robert-Moreno A, Pecoraro M, Ortells MC, Di Giacomo V, et al. Senescence is a developmental mechanism that contributes to embryonic growth and patterning. *Cell* **2013**, *155*, 1119–1130. DOI:10.1016/j.cell.2013.10.041
36. Yao H, Wallace J, Peterson AL, Scaffa A, Rizal S, Hegarty K, et al. Timing and cell specificity of senescence drives postnatal lung development and injury. *Nat. Commun.* **2023**, *14*, 273. DOI:10.1038/s41467-023-35985-4